LETTER

Enabling the Low-Temperature Cycling of NMC‖Graphite Pouch Cells with an Ester-Based Electrolyte

Yoon-Gyo Cho,[†] Mingqian Li,[†] John Holoubek,[†] Weikang Li, Yijie Yin, Ying Shirley Meng, and Zheng Chen*

Read Online

ACCESS | 📊 Metrics & More | 📖 Article Recommendations | 🆂🆅 Supporting Information

ABSTRACT: The operation of lithium-ion batteries (LIBs) at low temperatures ($\leq$−20 °C) is limited by reduced ionic transport properties of the electrolyte, as well as by severe charge-transfer polarization. Herein, we demonstrate that this low-temperature cycling limitation can be overcome in $LiNi_xMn_yCo_zO_2$ ($x + y + z = 1$) (NMC)‖graphite type full cells with a methyl propionate (MP)-based ester electrolyte. This electrolyte, consisting of $LiPF_6$ dissolved in MP and fluoroethylene carbonate (FEC), delivers successful cycling at the high rate of 0.5C at −20 °C. It also sustains stable charge and discharge cycling at −40 °C with 60% capacity retention compared with room-temperature operation. This outstanding electrochemical performance is further supported by electrochemical impedance spectroscopy (EIS) in three-electrode pouch cells to investigate the internal resistances between cathode and anode, as well as careful structure and composition characterizations at the electrode interfaces. This work offers a new avenue for high-performance LIBs capable of ultralow-temperature charging−discharging operation.
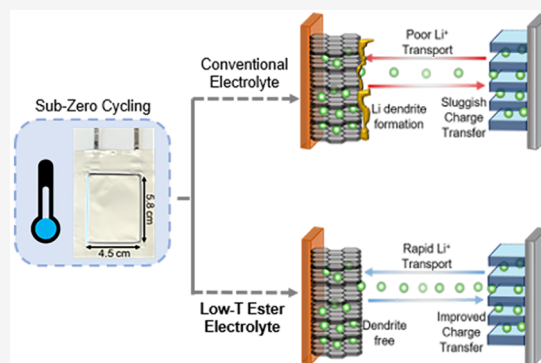
Lithium-ion batteries (LIBs) have been expanding their applications from the already commercialized mobile phones and laptop computers to electric vehicles (EVs) and energy storage systems (ESSs). In accordance with the diverse applications of LIBs, the cells should be able to maintain their energy and power densities under a wide range of operating temperatures.[1] However, typical LIBs containing carbonate-based conventional liquid electrolytes have suffered from various impedance issues such as ohmic resistance caused by poor electrolyte transport properties and sluggish charge transfer at the electrode interfaces.[2−4] These limitations are exacerbated at subzero temperatures because of insufficient ionic conductivity, freezing of the electrolyte, and sluggish Li^+ desolvation at the interphase, resulting in poor electrochemical performance.[5−7] As a representative example, it has been previously observed that full cells consisting of $Li_{1.2}Ni_{0.15}Co_{0.10}Mn_{0.55}O_2$‖graphite and carbonate-based electrolytes have produced only 28% of their room-temperature discharge capacity at a 0.1C rate and −20 °C.[8]

As these limitations stem from the electrolyte, improving the low-temperature electrochemical performance should also arise from the optimization of its components. Previous studies for enhancing the low-temperature operation of LIBs have been generally dedicated to (1) lowering the freezing point of the bulk

electrolyte to maintain a liquid phase at low-temperature in order to maintain sufficient ionic conductivity[9,10] and (2) forming low-resistance solid-electrolyte interface (SEI) layers on the anode side[11,12] and a cathode-electrolyte interface (CEI) layer on the cathode side[7,13] to reduce the resistance of the charge transfer and Li-ion (Li^+) diffusion through the interfaces.

Carboxylate esters have been previously considered as promising additive solvent candidates for low-temperature LIB electrolytes because of their beneficial physicochemical properties.[8,10,14] For instance, ethyl acetate (EA) was previously chosen because of its low freezing point (T_f) of −84 °C and a suitable dielectric constant of 6.02, which produced[15] a high ionic conductivity of 0.2 mS cm^{-2} at the ultralow temperature of −70 °C when paired with 1 M LiTFSI.[15] However, the cathodic stability was constrained to 1.5 V vs Li/Li^+, which indicates that this electrolyte is not capable of utilizing graphite as an anode.

Even though higher-concentration carboxylate ester-based electrolytes were able to expand the reduction stability to ∼0 V (Li/Li^{+}),[10] the compatability of such systems with full cell LIBs over long term cycles at low temperatures has been rarely reported.

Our recent work has demonstrated methyl propionate (MP) as a promising solvent for the low-temperature operation of graphite∥graphite dual-ion batteries (DIBs)[16] and Li-sulfurized polyacrylonitrile (Li∥SPAN) batteries.[17] While previous ester systems have been demonstrated, the acetate family has generally been attributed to poor reductive stability in addition to problematic high-temperature characteristics, while the butyrate class typically displays increased viscosities.[8,10] MP is particularly promising for low-temperature electrolytes because of its extremely low freezing temperature of −87.5 °C; relatively high boiling point of 79.8 °C; and low viscosity (0.43 cP), which is lower than that of dimethyl carbonate (DMC), 0.59 cP, the lowest viscosity of the conventional carbonate solvent family.[3] These physical properties of MP lead a high ionic conductivity at low temperature (Table S1). In addition, molecular dynamics (MD) simulation shows that the MP/FEC electrolyte system displays a solvation structure in which PF_6^- partially participates in the solvation, with calculated Li^{+}/solvent coordination number of 3.3, lower than the Li^{+}/solvent coordination number (3.7) in the 1 M LiPF₆ EC/DEC system.[7] This behavior is attributed to the partial participation of PF_6^- in the solvation, which is similar to the contact ion pair (CIP) solvation structure that is commonly associated with a high Li^{+} transference number and improved electrochemical stability at room temperature (RT).[18−20] However, to the best of our knowledge, the effect of such ester electrolyte chemistry on low-temperature charge and discharge behavior in NMC∥graphite type full cells has not been studied.

In this work, we report a major advance by demonstrating stable charge and discharge cycling of $LiNi_{0.33}Co_{0.33}Mn_{0.33}O_2$ (NMC111)∥graphite pouch-type full cells at temperature as low as −40 °C. Using the ester-based electrolyte consisting of MP:FEC (90:10 vol %) with 1 M LiPF₆, abbreviated as M9F1, we show significantly enhanced electrochemical cycling performance at −20 °C, far superior to the industry standard carbonate electrolytes. It also exhibits 60% capacity retention at −40 °C compared with RT charge and discharge operation. The outstanding electrochemical performance is further supported by electrochemical impedance spectroscopy (EIS) in three-electrode pouch cells to investigate the internal resistances between cathode and anode, as well as careful electrode interface characterizations. This work offers a new avenue for high-performance LIBs capable of ultralow-temperature charging−discharging operation.

First, it was found that the ionic conductivity (σ_i) of the M9F1 electrolyte is significantly improved compared with that of the conventional ethylene carbonate (EC)-based LP40 and LP30 electrolytes (LP40 = 1 M LiPF₆ in EC:DEC (5:5 vol %); LP30 = 1 M LiPF₆ in EC:DMC (5:5 vol %)), especially at temperatures below −20 °C (Figure 1a and Table S2). Specifically, the σ_i of M9F1 was found to be 2.48 mS cm^{−1} at −60 °C, whereas LP30 and LP40 showed sudden σ_i drop from −30 and 0 °C, respectively, which is typically related to the phase transition from liquid to solid of the electrolytes. Through the application of differential scanning calorimetry (DSC), it was found that M9F1 did not undergo a phase change between −90 and 50 °C, despite the relatively high freezing point of FEC (Figure 1b). However, LP30 displayed a freezing point at −21.9 °C, whereas
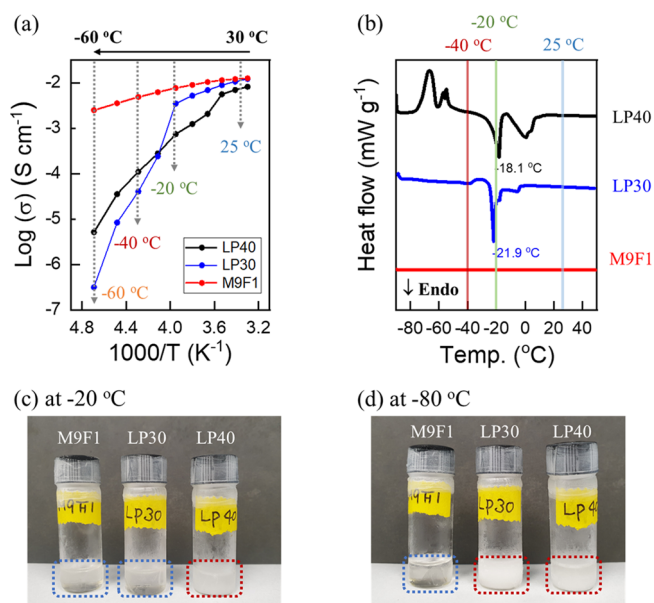
Figure 1. (a) Ionic conductivities (σ_i) of different electrolytes measured at various temperatures from −60 to 30 °C. The measurements of σ_i were recorded for each 10 °C. (b) Differential scanning calorimetry (DSC) heating curves of different electrolytes consisting of 1 M LiPF₆ for electrolyte phase confirmation. Samples were cooled to −90 °C and then heated up to 50 °C with 2 °C min^{−1}. Optical images of different electrolytes after storage for 12 h at −20 °C (c) or −80 °C (d). Electrolyte solution (1 mL) was added in each glass vial. Liquid phase and solid phase are indicated by blue and red rectangle boxes, respectively.

LP40 was found to exhibit two noticeable endothermic peaks at ∼0.5 °C as well as −18.1 °C. These phase transitions have been previously observed in the EC/DEC systems, where the initial peak corresponds to the initial solidification of EC, while we believe the secondary peak at −18.1 °C could be attributed to further internal ordering of the solid similar to a crystallization.[21,22] The single peak observed in the EC/DMC system is likely due to the significantly closer freezing points of the two solvents as compared to the large difference between EC and DEC (Table S1). The significantly steeper ionic conductivity degradation observed in LP30 is likely indicative of this trend, as liquid DEC is likely still present in the LP40 system below 0 °C (Figure 1a). These DSC results are also supported through observation of the electrolytes after storing at −20 and −80 °C for 12 h. As seen in Figures 1c,d and S1, LP40 and LP30 were found to freeze after storage at −20 and −40 °C, respectively, while M9F1 did not freeze even after days of storage at −80 °C.

On the basis of the outstanding ionic transport properties of M9F1, NMC111∥graphite pouch-type full cells were assembled for electrochemical performance assessment (Figures S2 and S3a,b). The discharge capacity of the cell was found to be 157.9 mAh g^{−1} (based on the cathode mass) for M9F1 with clear SEI formation peaks in the initial formation cycle, which was similar to the cells using LP30 and LP40 (Figure S3c,d). Next, the discharge rate capability test of the cells was assessed after charging all the cells at 0.1C to observe any variance in kinetic behavior between the electrolytes at room-temperature. It was found that M9F1 delivered a discharge capacity of 80 mAh g^{−1} at the discharge rate of 10C (Figures 2a,b and S4). Conversely, almost no discharge capacity was obtained for the cells with LP30 and LP40 under the same conditions. The rate capability of the M9F1 was also found to be significantly improved at 2C
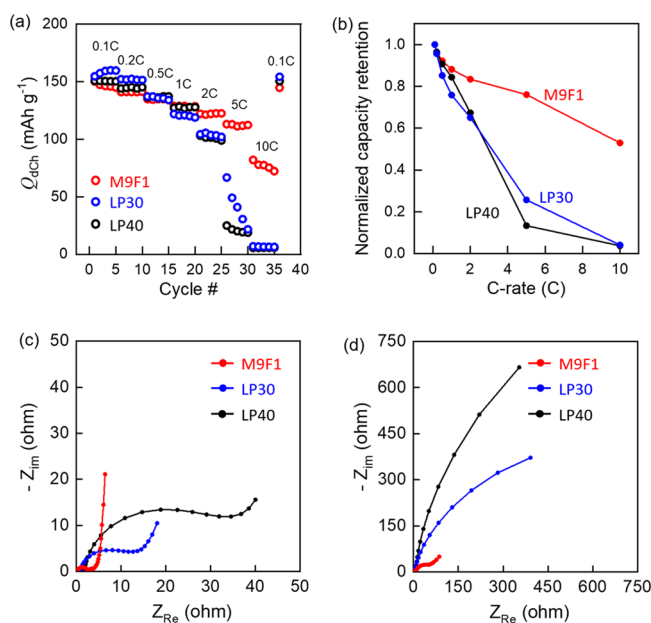
Figure 2. Rate performance results of the NMC111‖graphite pouch cells and EIS analysis data of the cell at 0% SOC after cycling. (a) Rate capabilities of full cells evaluated between 2.7 and 4.3 V voltage window using different electrolytes. All the cells have the same cathode and anode configuration, and the cell capacity was calculated and referred to the cathode mass. (b) The normalized capacity retention of panel a. The retentions are calculated from the discharge capacity of 0.1C. Nyquist plots of the cells after rate capabilities at the different temperature between (c) room-temperature (RT) and (d) −20 °C.

and 5C compared with LP30 and LP40. This phenomenon was further investigated by EIS measurement of the three discharged cells between RT and −20 °C at 0% stage of charge (SOC) (Figure 2c,d). The acquired full-cell impedance spectra can be distinguished by the bulk electrolyte resistance (R_s), SEI layer resistance (R_{SEI}), anode resistance (R_{ano}), and cathode resistance (R_{cat}) (Figure S5a).[23] During this analysis, it was found that the R_{cat} of the LP30 and LP40 was substantially higher than R_{ano} compared to the other resistances at both RT and −20 °C (Figure S5b,c). Furthermore, as seen in Figure 2d, the cathode resistances of LP30 and LP40 were remarkably increased at −20 °C compared with that at RT, which indicates that the charge-transfer resistance (R_{ct}) on the cathode is more limiting in this temperature range. This result suggests that the outstanding cycling at −20 °C may be caused by the extremely low charge-transfer resistance on the cathode provided by M9F1.

With the assessment of any prospective electrolyte for use in LIBs, it is also vital to address concerns regarding operational reversibility under standard conditions. As such, long cycling tests were conducted in NMC111‖graphite pouch-type full cells at room-temperature, where a capacity loss of only 0.6% was observed in the M9F1 cell over 300 cycles at 1C charge and discharge cycling, compared to 5.3% observed in the LP40 cell (Figure S6a). The M9F1 system was also found to provide similar advantages in the output voltage retention of the system, where the energy loss was found to be only 1.3% for the M9F1 system compared to 7.2% in LP40 (Figure S6b). Additionally, to provide a substantive result regarding the gas generation from the M9F1 system, three-layer pouch-type full cells were constructed and the gas volume was measured using the Arrhenius method (Supporting Information). It was found that
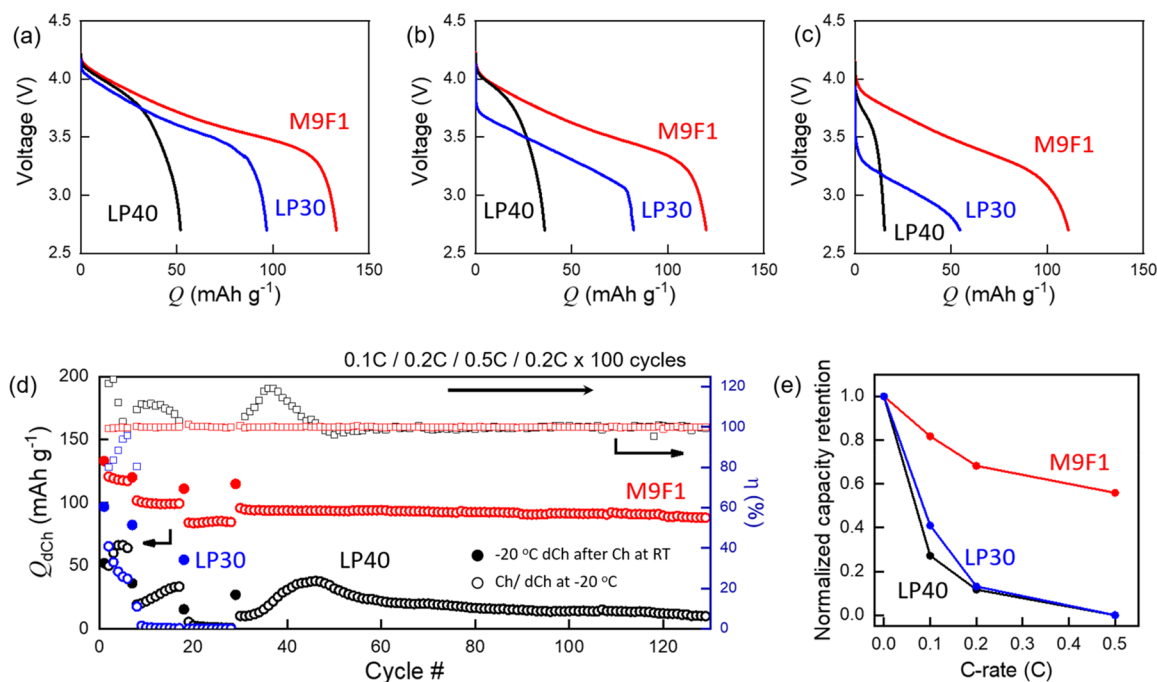
Figure 3. Low-temperature electrochemical performance of NMC111‖graphite type pouch cells using different electrolytes. Voltage profiles during discharge at (a) 0.1C, (b) 0.2C, and (c) 0.5C under −20 °C after room-temperature charge at 0.1C. (d) Charge and discharge cycling performance of cells at different C-rates (0.1C, 0.2C, and 0.5C) using different electrolytes. The cycling test was conducted on 0.1C for 5 cycles, 0.2C for 10 cycles, 0.5C for 10 cycles, and 0.2C for 100 cycles. The first closed circle at each C-rate is the first discharge capacity after charge at room-temperature. Following open circles are the repeated charge and discharge cycling after discharge at the same rate at −20 °C. (e) The normalized capacity retention at first charge from panel d.
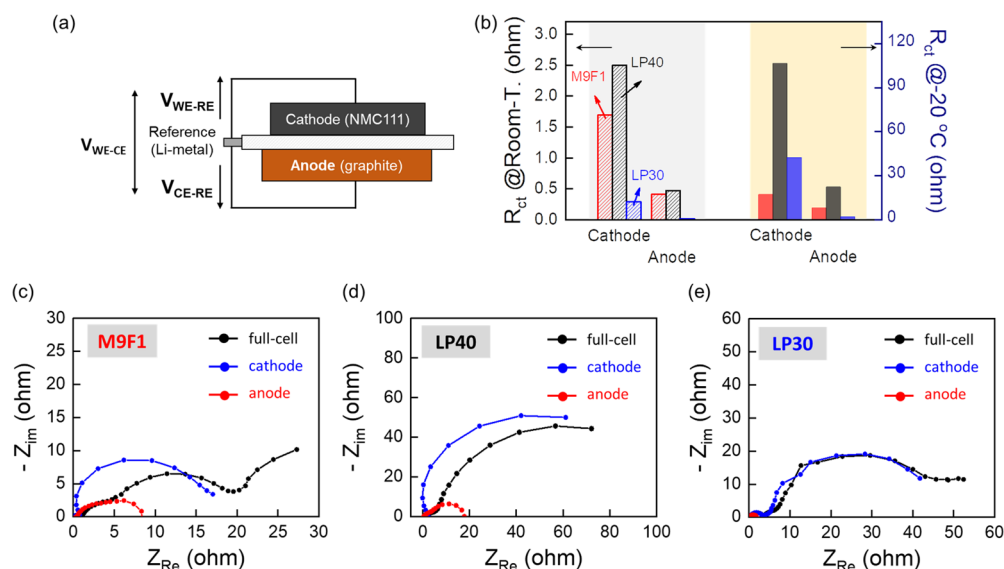
Figure 4. Cathode and anode impedance contributions from (a) the three-electrode pouch cell system. (b) The comparison of charge-transfer resistance (R_{ct}) of the cells using different electrolytes at the temperatures between room-temperature and −20 °C (red = M9F1, black = LP40, blue = LP30). Nyquist impedance plots of the cells using (c) M9F1, (d) LP40, and (e) LP30. Impedance of the cells were measured at 50% SOC. Impedance spectra was obtained with a frequency range between 1 mHz and 1 MHz.

after 8 cycles at 0.1C, the cell employing M9F1 ester electrolyte generated only 0.042 mL of gas compared to 0.1532 mL generated by the carbonate system (Figure S7 and Table S3). Crucially, the necessity of a 10% FEC content was also observed via the gassing and cycling comparison between the M9F1 system and a M95F5 formulation (MP:FEC = 95:5 in vol.), where the capacity was shown to sharply decay after only 5 cycles (Figure S8), generating 0.1933 mL of gas after 8 cycles (Table S3). These results not only indicate the practical viability of the M9F1 system for scale-up but also reveal the critical role of 10% FEC content in passivating the electrode surface, allowing for stable cycling and reduced gas generation.

NMC111‖graphite pouch-type full cells were then discharged at −20 °C after they were fully charged at RT and a 0.1C rate (Figure 3a−c). Despite similar IR drop behavior, the discharge capacity of M9F1 was found to retain 84% (133 mAh g^{-1}) of its RT capacity (Figure 3a), whereas the cells employing LP30 and LP40 displayed 61% and 33% of their RT capacity, respectively, under the same conditions. At the higher C-rate of 0.5C, the cell employing M9F1 delivered a discharge capacity retention of 70% (111 mAh g^{-1}) (Figure 3c). Although the M9F1 system's advantage was clearly shown during discharge, this electrolyte was also found to enable the cycling of these cells at −20 °C (Figure 3d). In Figure 3d, after an initial formation charge at RT (closed circle), both charge and discharge were conducted at each C-rate under −20 °C. Even at 0.1C, the cyclabilities of LP30 and LP40 faded dramatically in the first 5 cycles with significantly unstable Coulombic efficiencies (η). The capacity deterioration was more severe after charge and discharge rates were increased to 0.2C and 0.5C. Additionally, the LP30 and LP40 electrolytes did not exhibit any significant capacity at the aforementioned higher rates. In contrast, highly stable capacity retention was recorded at the same operating conditions in the cells employing M9F1. Assessing the last 100 cycles at 0.2C, 92% of the cell capacity was retained (i.e., 88 mAh g^{-1} for the 100th cycle, 95 mAh g^{-1} for the 1st cycle). The retained capacities at −20 °C and each C rate are summarized in Figure 3e to provide a clearer comparison. The results from these low-temperature

cycling experiments imply that the charging process of LIBs remains a monumental challenge that can be solved through the application of advanced electrolytes.

To further confirm the improved low-temperature performance of the cells containing M9F1 during operation, EIS measurements of three-electrode cells was carried out to record the resistances without influence from the counter electrode (CE).[24] In our system, a strip of lithium metal was used as the reference electrode (RE) in the pouch cells (Figure 4a), and the EIS was measured at 50% SOC after 5 cycles at 0.1C to ensure the stable formation of SEI and CEI layers. First, the R_{ct} of cathodes containing LP30 and LP40 was remarkably increased at −20 °C compared with that at RT, whereas M9F1 showed significant improvement over the other cells (Figures 4b−e and S9). The relatively increased R_{ct} of LP40-based cells may be caused by the solidification of the electrolyte at −20 °C as shown in Figure 1c. However, the R_{ct} of the anodes was found to be lower than that of the cathodes, which may suggest that the charge-transfer kinetics on the cathodes suffers more than that on the anodes at −20 °C (Table S4). On the other hand, M9F1 provided a significantly reduced cathode resistance, which may result from the stable interface film on the electrodes and the improved physical properties at low-temperature. This trend agrees with the full cell EIS analysis at 0% SOC (Figure 2c,d). Our finding is consistent with the recent study on the positive film-forming behavior of commercial size LiCoO$_2$‖graphite cells employing electrolytes with an FEC additive, which suggests that the impedance of R_{SEI} and R_{ct} is mainly distributed on the cathode side and that FEC plays a beneficial role.[13]

Three-electrode cells were also investigated for low-temperature discharge capability, which is shown in Figure S10. It was found that the graphite's average polarization between room temperature and −20 °C was 171 and 122 mV for LP30 and M9F1, respectively. The NMC 111, on the other hand showed substantially increased polarizations of 677 and 241 mV for LP30 and M9F1, respectively, which supports the trends revealed by EIS. However, it is important to note that while the polarization of the graphite anode is indeed lower than the
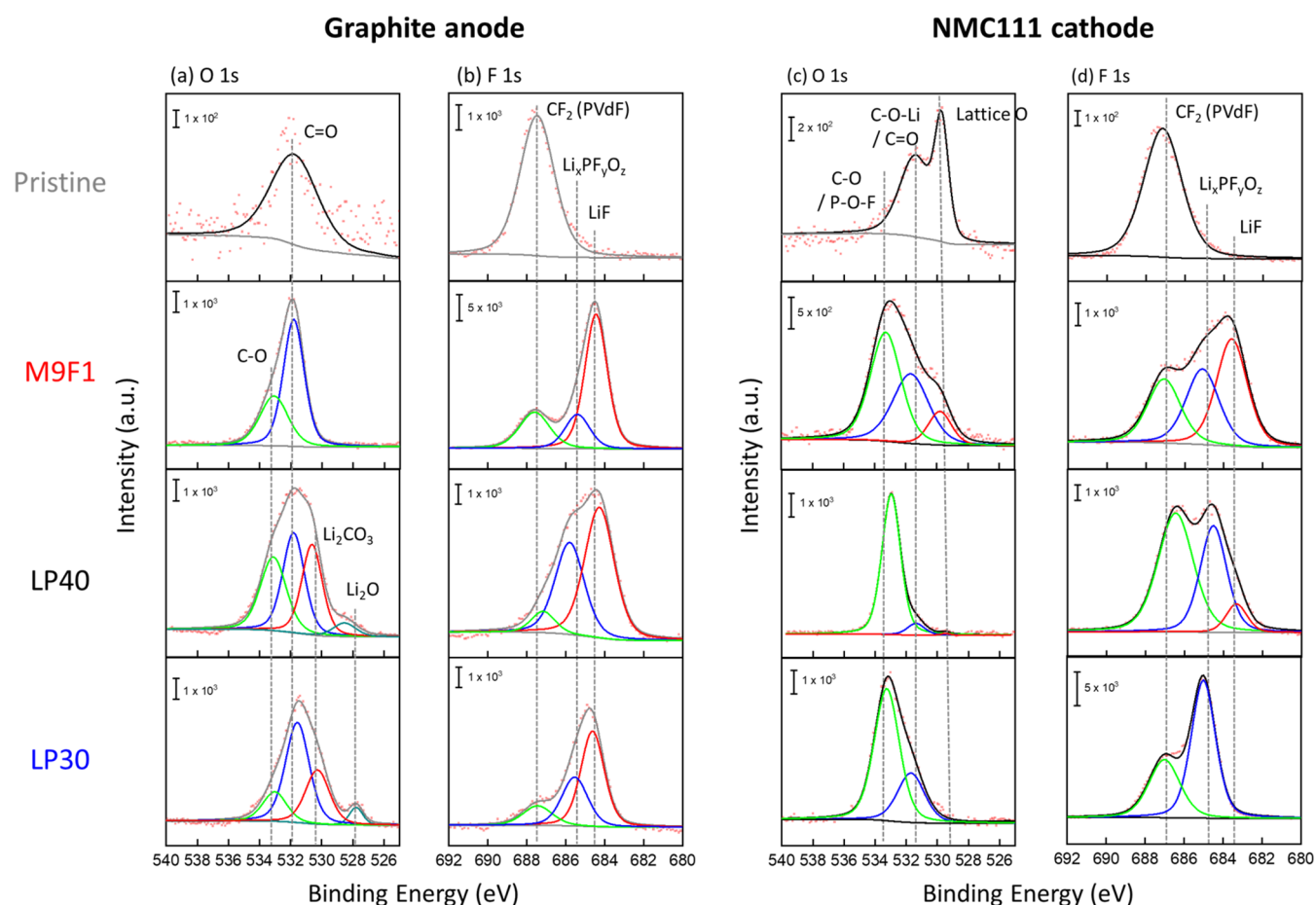
Figure 5. Characterization of electrode surfaces by XPS. (a) O 1s and (b) F 1s regions for graphite anodes; (c) O 1s and (d) F 1s regions for NMC111 cathodes. All the electrodes were obtained from cells after the cycling test described in Figure 3d.

NMC 111 cathode, its thermodynamic proximity to Li metal indicates that even small changes in the anode overpotential may result in Li metal plating.

X-ray photoelectron spectroscopy (XPS) was then conducted on the NMC111 cathodes and graphite anodes after cycling at −20 °C (Figure 3d) to probe the differences in interphase composition. As observed in the comparison of O 1s spectra (Figure 5a), electrolyte decomposition products of Li_2CO_3 (∼530.6 eV) and Li_2O (528.5 eV) were detected on the graphite anode cycled in LP40 and LP30 when compared to the pristine spectra. However, the graphite anode cycled in M9F1 reveals clear C=O (∼531.8 eV) and C−O (∼533.1 eV) peaks, which may suggest that the SEI layer formed by FEC and MP was largely free of $LiCO_3$ species. Further comparison with the F 1s spectra found in Figure 5b reveals a strong LiF peak at 684.5 eV in the spectra formed from M9F1, which could be formed from FEC or PF_6^- decomposition.[13] However, a relatively high ratio of $Li_xPF_yO_z$ was detected on the anode of LP40 and LP30, which may indicate the LiF produced in M9F1 is largely formed via FEC. It is worth noting that significant amounts of Li_2CO_3 and Li_2O have been previously associated with mixtures containing carbonate solvent molecules and may explain their absence in cathode interface with M9F1 electrolyte, which is composed largely of a carboxylate ester.[25]

From the viewpoint of cathode surface (Figure 5c), the significant species found in the O 1s spectra of M9F1 appear as C=O, C−O, and lattice oxygen at ∼533.3, ∼ 531.7, and ∼529.8 eV, respectively. In the presence of the LP30 and LP40

electrolytes, however, the peak for lattice oxygen disappeared with the high intensities of the other peaks. After the surface is etched for 120 s, however, the clear lattice oxygen peaks were obtained in the presence of LP30 and LP40 (Figure S11), which indicates that the CEI formed from these electrolytes was substantially thicker than that formed in M9F1 during cycling at −20 °C. As shown in Figure 5d, three peaks from the cathodes cycled in M9F1 are present in the F 1s spectra: (i) 683.6 eV ascribed to LiF, which is formed because of the electrochemical decomposition of FEC and $LiPF_6$; (ii) 685.1 eV assigned to $Li_xPF_yO_z$, indicative of $LiPF_6$ decomposition; and (iii) 687.1 eV responsible for CF_2 in the PVdF binder. However, the peak intensity of LiF was significantly decreased in the presence of LP40 and LP30 electrolyte with a significant increase of $Li_xPF_yO_z$, which indicates that most products of the CEI layer originated from the decomposition of $LiPF_6$ during cycling. We believe that the well-known effect of the thin and uniform LiF-rich SEI and CEI layers for electrochemical stability[26] would be beneficial even at low temperatures.

Furthermore, it was found that the resistive nature of the graphite anode encouraged lithium metal plating on the surface during low-temperature charging because of its increased polarization. The amount of deposited lithium and the speed of its growth can be controlled by (1) Li^+ transport limitations[27,28] and (2) the interphasial kinetic resistance due to its inhomogeneity,[29] which are exacerbated at subzero temperatures.[30−32] Through the application of scanning electron microscopy (SEM), it was observed that the graphite
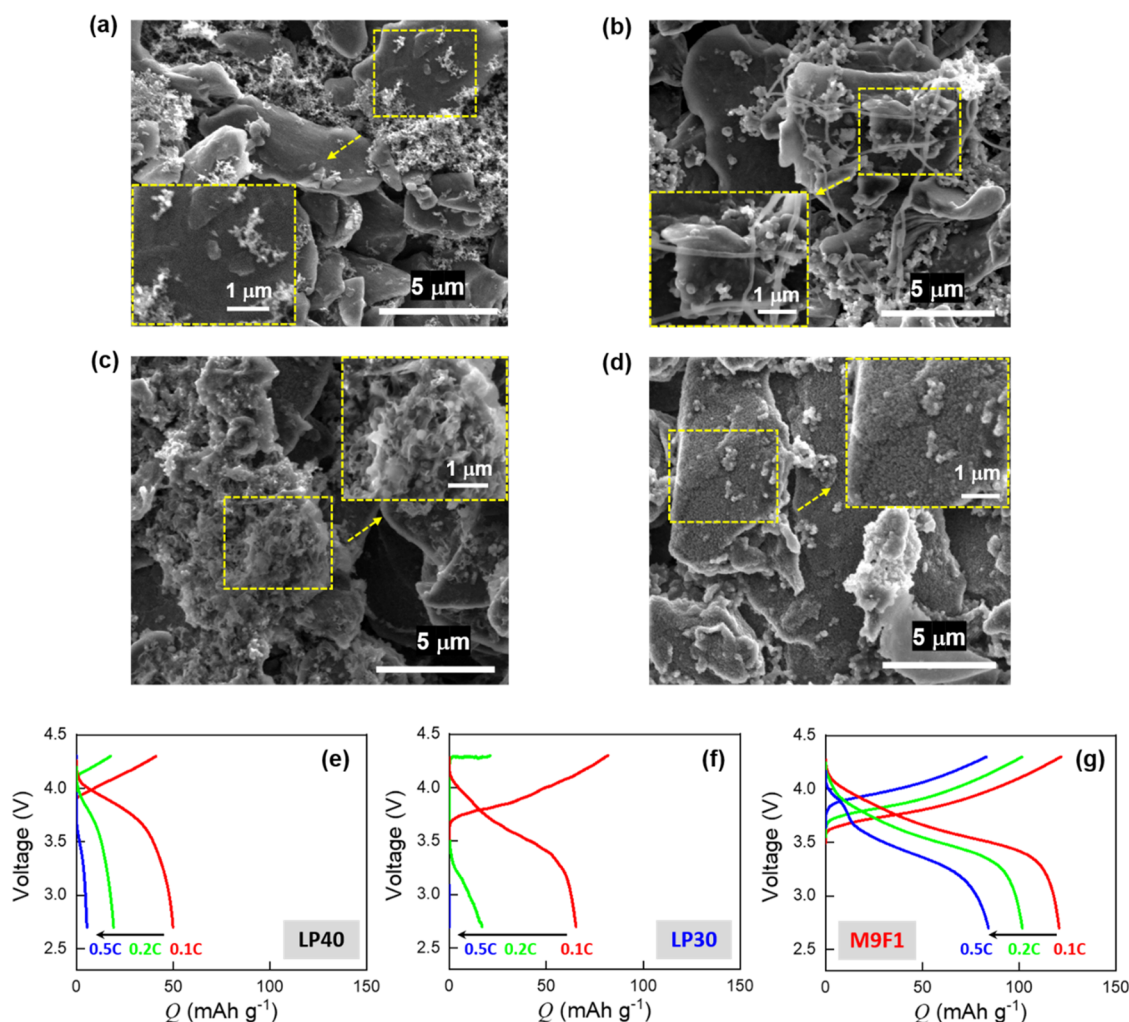
Figure 6. SEM images of the pristine and cycled graphite electrodes at −20 °C. All the cycled electrodes were obtained from cells after cycling test described in Figure 3d: (a) pristine graphite and graphite cycled in LP40 (b), LP30 (c), and M9F1(d). Potential profiles at the first charge and discharge cycle of cells with (e) LP40, (f) LP30, and (g) M9F1 electrolyte at −20 °C.

anodes cycled at −20 °C in LP30 and LP40 presented a significant amount of mossy and dendritic Li when compared with the pristine graphite (Figure 6a−c). The anode cycled in M9F1, however, did not show a significant Li metal presence (Figure 6d). The growth of Li metal at low temperatures is vital to avoid for both the safety and the cycling performance of LIBs. Because the highly reactive nature of Li leads to the loss of cyclable Li^+ and the growth and stripping of such metal lead to a significant increase in SEI, further increasing the polarization of the cell and reducing cell capacity (Figure 6e−g). This phenomenon is displayed in the Coulombic efficiency at −20 °C, where the LP30 system displayed an average CE of 94.4% when cycled at C/10, whereas the M9F1 system displayed an average CE of 99.5% (Figure 3d). It is also important to note that the presence of Li metal may lead to an increased initial discharge voltage due to the decreased potential of Li in relation to graphite. While this is ostensibly a performance improvement, the extremely diminished cycle life coincident with such plating events as well as the safety concerns associated with dendrites poses an extreme concern for LP30 and LP40 device operation at low temperatures. Though much higher capacity can be achieved by M9F1 electrolyte at low temperature, the small upper voltage plateau shown in the discharge curve at 0.5C from the M9F1 electrolyte indeed suggests the existence of Li

deposition on the anode during charging at low temperature (Figure 6g). Nevertheless, the relatively clean surface of the graphite particles with small roughness indicates that this insignificant amount of Li deposition is uniform (Figure 6d).

Though the advantage of the M9F1 electrolyte is clearly demonstrated at −20 °C, its ionic conductivity of 2.48 mS cm^{-1} of M9F1 at −60 °C indicates that this electrolyte may enable stable performance at even lower temperatures (Figure S12a). To demonstrate this, the pouch cells employing M9F1 were also cycled at −40 °C, which produced a discharge capacity of 109 mAh g^{-1} at a 0.1C rate (Figure S12). Furthermore, when cycled, the M9F1 cell was able to display a 94.5% and 96.3% capacity retention under 0.05C/0.05C, and 0.05C/0.1C of charge and discharge, respectively, as well as maintain stable Coulombic efficiencies. Note that LP30 and LP40 cells were not able to deliver any capacity because of poor transport properties and large electrolyte/electrode interfacial resistances at such a low temperature. Continuous improvement in the rate capability of NMC‖graphite type full cells for low-temperature charge and discharge cycling will need further work on the materials and electrode architecture design, which will be an important topic for our future study.

To enable wide-temperature battery operation that is of significant interest for broader applications, high-temperature

performance of the ester electrolyte should also be probed to provide a more wholistic system assessment. As such, we have assembled NMC 111‖graphite pouch-type full cells with different electrolytes and cycled them at 45 °C. As shown in Figure S13, after activation at room-temperature the M9F1 cell was able to maintain stable 1C cycling with no capacity degradation after 50 cycles at the elevated temperature. In contrast, the LP30 cell showed slightly lower initial capacity with an overall degradation of 4% at 1C. While the M95F5 cells show an initial capacity similar to that of the M9F1 cell at low rate, its capacity loss reached 10% after 50 cycles, indicating the important role of having a critical composition of FEC in the ester-based electrolyte. This result suggests that our ester electrolyte can be tailored for wide temperature range applications.

In summary, we successfully demonstrated that the capacity retention as well as Coulombic efficiency of NMC111‖graphite pouch-type full-cells was significantly improved in the presence of an MP-based ester electrolyte at the subzero temperatures of −20 and −40 °C. This aforementioned electrolyte was designed to endow ionic conductivity at low temperatures with an extremely low freezing point and LiF-rich interface layers on the cathode and anode, which facilitate charge transfer at both charge and discharge cycling. The 1 M $LiPF_6$ in MP:FEC electrolyte was effective in (1) enhancing the rate capability at room temperature and outstanding discharge properties at low-temperatures even at −40 °C and (2) protecting the cathode and anode by suppressing thick SEI layer formation and metallic Li deposition. We believe that this electrolyte formula can be used to improve the low-temperature performance of a variety of electrode chemistries and holds promise to do so at the pouch-cell level for more practical applications.

■ ASSOCIATED CONTENT

Ⓢ Supporting Information

The Supporting Information is available free of charge at https://pubs.acs.org/doi/10.1021/acsenergylett.1c00484.

> Experimental details; optical images of different electrolytes at different temperatures; SEM images; optical image of the assembled pouch cell; charge−discharge curves; voltage profiles of rate capability test; EIS spectra; room-temperature cycling stability; gassing investigation; three-electrode discharge profiles; XPS characterization of electrode surfaces; low- and high-temperature cycling stability test; physical properties of organic solvents (Table S1); summary of ionic conductivities (Table S2); gassing measurement of pouch cells with different electrolytes (Table S3); fitting values for the impedance spectra for 3-electrode pouch cells (Table S4) (PDF)

> Single- and multi-layer pouch cell setups for high-temperature cycling (XLSX)

■ AUTHOR INFORMATION

Corresponding Author

Zheng Chen − *Department of NanoEngineering, Program of Chemical Engineering, Program of Materials Science and Engineering, and Sustainable Power and Energy Center, University of California, San Diego, La Jolla, California 92093, United States;* ⓞ orcid.org/0000-0002-9186-4298; Email: zhengchen@eng.ucsd.edu

Authors

Yoon-Gyo Cho − *Department of NanoEngineering, University of California, San Diego, La Jolla, California 92093, United States*

Mingqian Li − *Program of Chemical Engineering, University of California, San Diego, La Jolla, California 92093, United States*

John Holoubek − *Department of NanoEngineering, University of California, San Diego, La Jolla, California 92093, United States;* ⓞ orcid.org/0000-0003-0015-4512

Weikang Li − *Department of NanoEngineering, University of California, San Diego, La Jolla, California 92093, United States*

Yijie Yin − *Program of Materials Science and Engineering, University of California, San Diego, La Jolla, California 92093, United States*

Ying Shirley Meng − *Department of NanoEngineering, Program of Materials Science and Engineering, and Sustainable Power and Energy Center, University of California, San Diego, La Jolla, California 92093, United States;* ⓞ orcid.org/0000-0001-8936-8845

Complete contact information is available at:
https://pubs.acs.org/10.1021/acsenergylett.1c00484

Author Contributions

†Y.-G.C., M.L., and J.H. contributed equally to this work.

Notes

The authors declare the following competing financial interest(s): A Patent Disclosure related to this work is under processing through the UCSD Office of Innovation & Commercialization.

■ ACKNOWLEDGMENTS

■ REFERENCES

(1) Hou, J.; Yang, M.; Wang, D.; Zhang, J. Fundamentals and Challenges of Lithium Ion Batteries at Temperatures between− 40 and 60 °C. *Adv. Energy Mater.* **2020**, *10* (18), 1904152.

(2) Liu, Y.; Zhu, Y.; Cui, Y. Challenges and opportunities towards fast-charging battery materials. *Nature Energy* **2019**, *4* (7), 540−550.

(3) Xu, K. Nonaqueous liquid electrolytes for lithium-based rechargeable batteries. *Chem. Rev.* **2004**, *104* (10), 4303−4418.

(4) Xu, K. Electrolytes and interphases in Li-ion batteries and beyond. *Chem. Rev.* **2014**, *114* (23), 11503−11618.

(5) Zhang, S.; Xu, K.; Jow, T. Low-temperature performance of Li-ion cells with a $LiBF_4$-based electrolyte. *J. Solid State Electrochem.* **2003**, *7* (3), 147−151.

(6) Sazhin, S. V.; Khimchenko, M. Y.; Tritenichenko, Y. N.; Lim, H. S. Performance of Li-ion cells with new electrolytes conceived for low-temperature applications. *J. Power Sources* **2000**, *87* (1−2), 112−117.

(7) Holoubek, J.; Yu, M.; Yu, S.; Li, M.; Wu, Z.; Xia, D.; Bhaladhare, P.; Gonzalez, M. S.; Pascal, T. A.; Liu, P.; et al. An All-Fluorinated Ester Electrolyte for Stable High-Voltage Li Metal Batteries Capable of Ultra-

Low-Temperature Operation. *ACS Energy Letters* **2020**, 5 (5), 1438−1447.

(8) Smart, M. C.; Ratnakumar, B. V.; Surampudi, S. Use of Organic Esters as Cosolvents in Electrolytes for Lithium-Ion Batteries with Improved Low Temperature Performance. *J. Electrochem. Soc.* **2002**, *149*, A361.

(9) Cho, Y.-G.; Kim, Y.-S.; Sung, D.-G.; Seo, M.-S.; Song, H.-K. Nitrile-assistant eutectic electrolytes for cryogenic operation of lithium ion batteries at fast charges and discharges. *Energy Environ. Sci.* **2014**, 7 (5), 1737−1743.

(10) Dong, X.; Lin, Y.; Li, P.; Ma, Y.; Huang, J.; Bin, D.; Wang, Y.; Qi, Y.; Xia, Y. High-energy rechargeable metallic lithium battery at− 70 °C enabled by a cosolvent electrolyte. *Angew. Chem.* **2019**, *131* (17), 5679−5683.

(11) Liao, L.; Zuo, P.; Ma, Y.; An, Y.; Yin, G.; Gao, Y. Effects of fluoroethylene carbonate on low temperature performance of mesocarbon microbeads anode. *Electrochim. Acta* **2012**, *74*, 260−266.

(12) Xu, G.; Huang, S.; Cui, Z.; Du, X.; Wang, X.; Lu, D.; Shangguan, X.; Ma, J.; Han, P.; Zhou, X.; et al. Functional additives assisted ester-carbonate electrolyte enables wide temperature operation of a high-voltage (5 V-Class) Li-ion battery. *J. Power Sources* **2019**, *416*, 29−36.

(13) Liu, D.; Qian, K.; He, Y.-B.; Luo, D.; Li, H.; Wu, M.; Kang, F.; Li, B. Positive film-forming effect of fluoroethylene carbonate (FEC) on high-voltage cycling with three-electrode LiCoO$_2$/Graphite pouch cell. *Electrochim. Acta* **2018**, *269*, 378−387.

(14) Logan, E. R.; Hall, D. S.; Cormier, M. M.; Taskovic, T.; Bauer, M.; Hamam, I.; Hebecker, H.; Molino, L.; Dahn, J. R. Ester-Based Electrolytes for Fast Charging of Energy Dense Lithium-Ion Batteries. *J. Phys. Chem. C* **2020**, *124*, 12269−12280.

(15) Dong, X.; Guo, Z.; Guo, Z.; Wang, Y.; Xia, Y. Organic batteries operated at− 70 °C. *Joule* **2018**, *2* (5), 902−913.

(16) Holoubek, J.; Yin, Y.; Li, M.; Yu, M.; Meng, Y. S.; Liu, P.; Chen, Z. Exploiting Mechanistic Solvation Kinetics for Dual-Graphite Batteries with High Power Output at Extremely Low Temperature. *Angew. Chem., Int. Ed.* **2019**, *58* (52), 18892−18897.

(17) Cai, G.; Holoubek, J.; Xia, D.; Li, M.; Yin, Y.; Xing, X.; Liu, P.; Chen, Z. An ester electrolyte for lithium−sulfur batteries capable of ultra-low temperature cycling. *Chem. Commun.* **2020**, *56* (64), 9114−9117.

(18) Suo, L.; Borodin, O.; Gao, T.; Olguin, M.; Ho, J.; Fan, X.; Luo, C.; Wang, C.; Xu, K. "Water-in-Salt" Electrolyte Enables High-Voltage Aqueous Lithium-Ion Chemistries. *Science* **2015**, *350* (6263), 938−943.

(19) Chen, S.; Zheng, J.; Mei, D.; Han, K. S.; Engelhard, M. H.; Zhao, W.; Xu, W.; Liu, J.; Zhang, J.-G. High-Voltage Lithium-Metal Batteries Enabled by Localized High-Concentration Electrolytes. *Adv. Mater.* **2018**, *30* (21), 1706102.

(20) Suo, L.; Xue, W.; Gobet, M.; Greenbaum, S. G.; Wang, C.; Chen, Y.; Yang, W.; Li, Y.; Li, J. Fluorine-Donating Electrolytes Enable Highly Reversible 5-V-Class Li Metal Batteries. *Proc. Natl. Acad. Sci. U. S. A.* **2018**, *115* (6), 1156−1161.

(21) Ding, M. S.; Xu, K.; Jow, T. R. Liquid-Solid Phase Diagrams of Binary Carbonates for Lithium Batteries. *J. Electrochem. Soc.* **2000**, *147*, 1688.

(22) Ding, M. S.; Xu, K.; Zhang, S.; Jow, T. R. Liquid/Solid Phase Diagrams of Binary Carbonates for Lithium Batteries Part II. *J. Electrochem. Soc.* **2001**, *148*, A299.

(23) Momma, T.; Matsunaga, M.; Mukoyama, D.; Osaka, T. Ac impedance analysis of lithium ion battery under temperature control. *J. Power Sources* **2012**, *216*, 304−307.

(24) Raccichini, R.; Amores, M.; Hinds, G. Critical review of the use of reference electrodes in li-ion batteries: A diagnostic perspective. *Batteries* **2019**, *5* (1), 12.

(25) Delacourt, C.; Kwong, A.; Liu, X.; Qiao, R.; Yang, W.; Lu, P.; Harris, S.; Srinivasan, V. Effect of manganese contamination on the solid-electrolyte-interphase properties in Li-ion batteries. *J. Electrochem. Soc.* **2013**, *160* (8), A1099.

(26) Wang, C.; Meng, Y. S.; Xu, K. Perspective—fluorinating interphases. *J. Electrochem. Soc.* **2019**, *166* (3), A5184.

(27) Zhao, C.-Z.; Zhang, X.-Q.; Cheng, X.-B.; Zhang, R.; Xu, R.; Chen, P.-Y.; Peng, H.-J.; Huang, J.-Q.; Zhang, Q. An anion-immobilized composite electrolyte for dendrite-free lithium metal anodes. *Proc. Natl. Acad. Sci. U. S. A.* **2017**, *114* (42), 11069−11074.

(28) Chen, L.; Li, Y.; Li, S.-P.; Fan, L.-Z.; Nan, C.-W.; Goodenough, J. B. PEO/garnet composite electrolytes for solid-state lithium batteries: from "ceramic-in-polymer" to "polymer-in-ceramic. *Nano Energy* **2018**, *46*, 176−184.

(29) Hao, F.; Verma, A.; Mukherjee, P. P. Mechanistic insight into dendrite−SEI interactions for lithium metal electrodes. *J. Mater. Chem. A* **2018**, *6* (40), 19664−19671.

(30) Bugga, R. V.; Smart, M. C. Lithium plating behavior in lithium-ion cells. *ECS Trans.* **2009**, *25* (36), 241.

(31) Love, C. T.; Baturina, O. A.; Swider-Lyons, K. E. Observation of lithium dendrites at ambient temperature and below. *ECS Electrochem. Lett.* **2015**, *4* (2), A24.

(32) Wang, S.; Rafiz, K.; Liu, J.; Jin, Y.; Lin, J. Y. Effects of lithium dendrites on thermal runaway and gassing of LiFePO$_4$ batteries. *Sustainable Energy & Fuels* **2020**, *4* (5), 2342−2351.